

## Controlling the spectral shape of nonlinear Thomson scattering with proper laser chirping

S. G. Rykovanov,<sup>\*</sup> C. G. R. Geddes, C. B. Schroeder, E. Esarey, and W. P. Leemans

*Lawrence Berkeley National Laboratory, Berkeley, California 94720, USA*

(Received 8 December 2014; revised manuscript received 9 December 2015; published 18 March 2016)

Effects of nonlinearity in Thomson scattering of a high intensity laser pulse from electrons are analyzed. Analytic expressions for laser pulse shaping in frequency (chirping) are obtained which control spectrum broadening for high laser pulse intensities. These analytic solutions allow prediction of the spectral form and required laser parameters to avoid broadening. Results of analytical and numerical calculations agree well. The control over the scattered radiation bandwidth allows narrow bandwidth sources to be produced using high scattering intensities, which in turn greatly improves scattering yield for future x- and gamma-ray sources.

DOI: 10.1103/PhysRevAccelBeams.19.030701

### I. INTRODUCTION

Scattering of laser light from fast moving electrons is a widely used source of x- and gamma-ray photons [1–22]. Note that this process is widely known as inverse Compton scattering, but as the recoil is neglected throughout this paper, we refer to it as Thomson scattering (TS). Limits of validity of such a classical approach are discussed in detail in Sec. II. Applications of TS include photon sources of percent-level bandwidth for nuclear resonance fluorescence or photofission ([23–27] and references therein), for radiography [28,29] and for medical applications [30,31]. Thomson sources' monochromaticity, wide-range tunability (depending on the energy of the electrons in the beam) and directionality provide important advantages over Bremsstrahlung sources.

Applications of Thomson sources require high photon fluxes, which is challenging due to the small Thomson cross section. The total number of electrons,  $N_e$ , that can be accelerated in a bunch is limited for the high quality bunches required to produce narrow bandwidth sources. For example, laser plasma accelerators produce typically near  $N_e \sim 10^8$  [32], and conventional linacs are typically in the same range for low emittances [33]. Scattering laser performance and geometry are then principal tools for achieving the required fluxes. The produced photon yield is proportional to the product of  $N_e$  with the scattering laser intensity and pulse length. The need to match the laser diffraction range to its pulse length (to keep intensity

constant over the scattering volume) has meant that increasing yield by increasing laser pulse length costs quadratically in laser energy. For example, to double yield at constant intensity, pulse length must double and diffraction range must also double, requiring the spot size to increase by  $\sqrt{2}$ , requiring a fourfold increase in scatter laser energy. This makes it desirable to scatter at high laser intensity in order to maximize yield at reasonable laser energy cost.

Scattering laser intensity is strongly limited by the fact that the generated spectrum can be broadened and a bandlike structure can appear in the fundamental frequency as well as its harmonics [34–46] even for rather low values of laser pulse amplitude  $a_0 = \tilde{e}\tilde{A}_L/\tilde{m}_e\tilde{c}^2$  on the order of  $a_0 > 0.1$ , where  $\tilde{e}$  and  $\tilde{m}_e$  are absolute value of charge and mass of the electron respectively,  $\tilde{c}$  is the speed of light in vacuum and  $\tilde{A}_L$  is the laser vector potential amplitude in Gaussian cgs units. This is a detrimental and limiting effect in the cases when a narrow bandwidth gamma or x-ray sources are essential, especially in the case of nuclear resonance fluorescence for active nuclear interrogation. It puts a limit on the maximum laser intensity and thus maximum laser pulse amplitude  $a_0$  that can be used for obtaining a certain full width at half maximum (FWHM) bandwidth of the photon source. For example, such moderate laser pulse amplitude as  $a_0 = 0.2$  already leads to broadening on the order of 4%. The limit on intensity is an important driver of the laser energy and hence cost of a Thomson source [27]: producing one photon per electron costs 1.6 Joules of laser energy at  $a_0 = 0.15$ , but only 0.4 J at  $a_0 = 0.3$ .

Limited sets of parameters have been found to minimize the nonlinear effects, mainly based on shaping of the laser pulse temporal envelope. Hartemann *et al.* [38] showed that a flattop longitudinal intensity profile could reduce the effects of nonlinearity, but this approach is typically limited by the diffraction range of the laser pulse. In fact,

<sup>\*</sup>Present address: Helmholtz-Institut Jena, Fröbelstieg 3, 07743, Jena, Germany.  
S.Rykovanov@gsi.de

Published by the American Physical Society under the terms of the Creative Commons Attribution 3.0 License. Further distribution of this work must maintain attribution to the author(s) and the published article's title, journal citation, and DOI.

free-electron lasers (FELs) work using undulators with constant strength parameters  $a_0$  on the order of unity for optimal photon yield. Three-dimensional effects that appear due to tight laser pulse focusing can be also detrimental in TS as discussed by Hartemann *et al.* [36]. Ideally one would need laser pulses having near flat-top distribution in all dimensions. Ghebregziabher *et al.* [35] have proposed controlling the shape of the photon spectrum using laser pulse chirping and demonstrated it using a single set of numerical simulations. Such simulations have been extended both numerically and analytically by Terzić *et al.* [47]. There is however need for an analytical framework and solutions for nonlinear broadening, spectral shape, and compensation of these effects using laser pulse shaping in frequency (chirping) to obtain narrow bandwidth.

In this manuscript we derive analytical expressions for the spectrum of the nonlinear Thomson scattering for both cases of unchirped and chirped pulses and compare them to the results of numerical integration. We demonstrate that proper laser pulse chirping leads to bandwidth narrowing for large laser pulse amplitudes. This allows design of sources for narrow bandwidth together with high efficiency, without scanning of numerical parameters. The paper is organized as follows. In Sec. II a physical explanation of the spectrum broadening and appearance of substructures in the spectrum is provided. Analytical expressions for the nonlinear Thomson scattering spectrum are derived and compared with the results of numerical integration. In Sec. III this analysis is extended to show that the laser frequency-versus-time dependence, or chirp, can be used to compensate for nonlinear effects and to narrow the spectrum even for high intensity lasers. Finally, discussions and conclusions are presented in Sec. IV.

## II. NONLINEAR BROADENING AND SPECTRAL SHAPE

Spectral broadening and appearance of substructures due to the nonlinear effects in Thomson scattering have been reported in several previous works [34,35,37–40,43–45,47]. The appearance of substructures was identified to be due to constructive and destructive interference of radiation emitted from different electron positions within the scattering laser pulse. Here we begin by reviewing this physical explanation of the shape of the spectrum, then derive the shape of the spectrum analytically and compare it to that obtained via numerical integration. In addition to providing analytic derivation of the spectrum, this will serve as the basis for the derivation of compensation techniques required to produce narrow bandwidth at high intensity.

Let us first describe the limits of validity of the model that we have used throughout this paper. First, we have neglected the recoil on the electron due to the emission of a single photon. This is valid when the recoil parameter satisfies  $\zeta = 2\gamma\tilde{E}_p a_0 / \tilde{m}_e \tilde{c}^2 \ll 1$ , as discussed in the

pioneering paper by Nikishov and Ritus [48]. Here,  $\gamma$  is the relativistic Lorentz factor of an electron and  $\tilde{E}_p$  is the energy of the incoming photon in the laboratory frame (i.e., 1.55 eV for 0.8  $\mu\text{m}$  wavelength). For example, for a 1 GeV electron colliding head-on with a 1.55 eV photon, the recoil parameter  $\zeta \approx 0.01a_0$  and, hence, can be neglected if  $a_0 \ll 100$ . Another effect that has been neglected throughout this paper is the radiation friction that occurs due to the energy loss during multiphoton emission. Radiation friction can be neglected for  $a_0 < \epsilon_{\text{rad}}^{-1/3}$ , where  $\epsilon_{\text{rad}} = 2\gamma \frac{4\pi}{3} \frac{\tilde{r}_e}{\tilde{\lambda}_L}$  is the radiation parameter with  $\tilde{r}_e$  the classical electron radius and  $\tilde{\lambda}_L$  is the laser pulse wavelength [49]. For a 1 GeV electron interacting with a laser pulse with a wavelength  $\tilde{\lambda}_L = 0.8 \mu\text{m}$ , radiation friction can be neglected for  $a_0 < 25$ . The classical electrodynamic model that is used throughout this paper is valid for a vast parameter range, especially for the parameters of interest for applications, which typically require  $a_0 \sim 1$  [27].

We work in the frame of reference where an electron is initially at rest and the plane electromagnetic laser wave impinges it. Results presented can be immediately applied to the case of scattering from the electron moving with high speed (e.g., a relativistic electron beam) by using a Lorentz transform. We use a circularly polarized scattering laser pulse as it allows us to obtain analytical expressions for the spectrum similar to solutions derived by Hartemann *et al.* [38]. In terms of number of generated photons there is no difference for the case of pulses with different polarizations with same energy. The case of linear polarization can be modeled in a straightforward way using numerical integration [35,39].

Consider the case of a circularly polarized laser pulse with constant amplitude  $a_0$  impinging on an electron initially at rest. The central frequency of the on-axis reflected radiation spectrum is given by

$$\omega_c = \frac{1}{1 + a_0^2}, \quad (1)$$

where  $\omega_c = \tilde{\omega}_c / \tilde{\omega}_L$  with  $\tilde{\omega}_c$  and  $\tilde{\omega}_L$  being the reflected radiation and laser frequencies, respectively. Here and further in the paper, quantities with a tilde are given in the Gaussian cgs units, and quantities without a tilde are dimensionless. In these dimensionless units, frequency  $\omega$  is measured in terms of laser pulse frequency  $\tilde{\omega}_L$ . Equation (1) can be understood by calculating the frequency generated on axis by an electron with large  $\gamma$ , which is then given by the well-known formula  $\omega_c = 4\gamma^2 / (1 + a_0^2)$ . Performing the Lorentz transformation to the frame where the electron is at rest, one obtains Eq. (1). The convention used in this paper is that a circularly polarized laser pulse has twice the energy of a linearly polarized laser pulse with the same  $a_0$ , so that in the case of linear polarization the frequency is given by  $\omega_c = \frac{1}{1 + a_0^2/2}$ . The  $a_0^2$  term in the denominator comes from the fact that an electron is pushed by the

electromagnetic wave in the direction of its propagation by the  $\mathbf{v} \times \mathbf{B}$  force, and thus moves away from the laser pulse redshifting the reflected light.

Movement of the electron through the focus of the laser and/or pulsing of the laser beam means that the electron does not always experience the peak value of the laser pulse  $a_0$ . Hence, in Eq. (1),  $a_0$  must be multiplied by a function of running time  $g(\eta)$  describing the laser pulse envelope. Here,  $\eta = \tilde{\omega}_L(\tilde{t} - \tilde{z}/\tilde{c})$  and  $z = \frac{\tilde{\omega}_L}{c}\tilde{z}$  with  $\tilde{t}$  and  $\tilde{z}$  being time and longitudinal coordinate, respectively, and it is assumed that the laser pulse impinges the electron from the left side. The laser pulse vector potential envelope is then described by a function of time  $a(\eta) = a_0g(\eta)$ . This leads to the following equation for the reflected radiation central frequency:

$$\omega_c(\eta) = \frac{1}{1 + a(\eta)^2}. \quad (2)$$

Therefore, during the laser pulse interaction with an electron, different frequencies are generated at different times and different electron positions within the envelope. As a result, the reflected radiation spectrum is considerably broadened in the case of a strong laser pulse with a varying laser envelope. Additionally, a bandlike structure appears in the reflected spectrum as shown in Fig. 1 (left) for  $a_0 = 0.4$ , as compared with the linear case  $a_0 \ll 1$  (in this case  $a_0 = 0.05$ ). For this calculation, we have used a laser pulse with an envelope described by Eq. (12). Qualitatively, broadening and band-structure appearance for strong laser pulses is illustrated in Fig. 1 (right), where the laser pulse envelope  $a(\eta)$ , generated frequency  $\omega_c(\eta)$  and electron longitudinal electron coordinate  $z(\eta)$  are schematically shown as functions of running time  $\eta$ . One can see that certain frequencies are generated twice during the interaction. For example, the frequency  $\omega_1$  is generated at two different longitudinal positions of the electron  $z_1$  and  $z_2$  as shown with black color in Fig. 1 (right). Depending on the

value of  $\omega_1$  and the separation between the emission points this leads to either constructive or destructive interference in the generated spectrum. These interference patterns lead to the appearance of bands in the spectrum.

The number of oscillations in the spectrum can be approximately established as a ratio of maximum frequency broadening due to laser intensity derived from Eq. (2) and given by  $\Delta\tilde{\omega} = \tilde{\omega}_L - \frac{\tilde{\omega}_L}{1+a_0^2}$  and the bandwidth of the laser pulse. Thus, the number of oscillations is roughly given by

$$N_{\text{osc}} = \tilde{\omega}_L \frac{a_0^2}{1 + a_0^2} \frac{1}{\Delta\tilde{\omega}_L}, \quad (3)$$

where  $\Delta\tilde{\omega}_L$  is the FWHM bandwidth of the laser pulse. One can see that the number of interference fringes in the spectrum grows with increasing laser amplitude and laser pulse duration (as laser pulse bandwidth is inversely proportional to laser duration).

The exact shape of the spectrum depends on the laser pulse duration and on its envelope shape and intensity, and can be calculated from the well-known motion of a free electron in a plane electromagnetic wave [17,50,51]. Here, we neglect the radiation friction so that the electron dynamics is governed by the standard Lorentz force. For an electron initially at rest and for an electromagnetic wave impinging the electron from the  $z \rightarrow -\infty$ , one can immediately write two integrals of motion:

$$u_{\perp} = a_{\perp} \quad (4)$$

$$\gamma - u_z = 1. \quad (5)$$

The latter equation can be also written in the following form:

$$u_z = \frac{a_{\perp}^2}{2}. \quad (6)$$

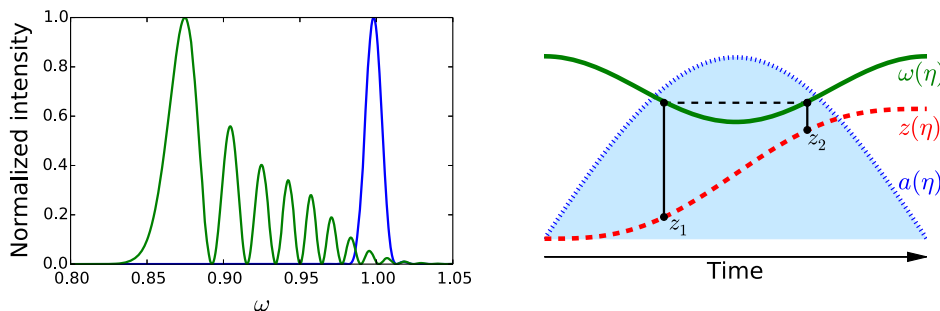


FIG. 1. Left: An example of the normalized on-axis spectra of reflected radiation calculated for low  $a_0 = 0.05$  (blue line) and high  $a_0 = 0.4$  (red color) scattering lasers, demonstrating the appearance of bandlike structure in the spectrum. Right: Qualitative illustration of the broadening and band formation mechanism in the nonlinear response of an electron to a strong electromagnetic wave. A laser pulse impinges the electron from the left side (from  $z \rightarrow -\infty$ ). As functions of time, the blue line and shaded area represent the laser pulse envelope, the green line shows the frequency of the reflected wave in accordance with Eq. (2), and the red dashed line shows the longitudinal coordinate of the electron.

Here, the dimensionless quantities:  $u_{\perp} = \frac{\tilde{p}_{\perp}}{m_e c}$  is any electron momentum component perpendicular to the  $z$ -axis,  $a_{\perp}$  is any perpendicular component of the normalized laser pulse vector potential, and  $u_z = \frac{\tilde{p}_z}{m_e c}$  is the electron longitudinal momentum component. Similarly,  $\tilde{p}_{\perp}$  and  $\tilde{p}_z$  are perpendicular and longitudinal electron momentum components in Gaussian cgs units, respectively.

For the observer looking on axis, the retarded time used for calculating the spectrum [50,51] does not depend on  $x$  and  $y$  coordinates. Hence, to derive the on-axis spectrum one only needs to know the  $z$  coordinate of the electron, which can be found from the following equation:

$$\frac{dz}{d\eta} = u_z \quad (7)$$

or, equivalently,

$$z(\eta) = \int_{-\infty}^{\eta} u_z(\eta') d\eta' = \int_{-\infty}^{\eta} \frac{a_{\perp}(\eta')^2}{2} d\eta'. \quad (8)$$

Since the trajectory of the electron in a plane electromagnetic wave is completely known, the on-axis reflected radiation produced by the electron moving in such a wave can be found using the well-known formula [50,51]:

$$\left. \frac{d^2 \tilde{I}}{d\omega d\Omega} \right|_{\theta=0} = \tilde{\kappa} \frac{\omega^2}{4\pi^2} \left| \int_{-\infty}^{+\infty} \mathbf{n} \times [\mathbf{n} \times \mathbf{u}_{\perp}(\eta)] e^{i\omega[\eta+2z(\eta)]} d\eta \right|^2, \quad (9)$$

where  $\tilde{I}$  is radiated energy in ergs,  $\Omega$  is the solid angle and the whole formula is evaluated for the on-axis case ( $\theta = 0$ ),  $\tilde{\kappa} = \frac{e^2 \tilde{\omega}_L}{c}$  is the normalization coefficient [such that both parts of Eq. (9) are measured in ergs] and  $\mathbf{u}_{\perp}$  is the vector of perpendicular momentum components. Using Eqs. (4) and (8) one can rewrite Eq. (9) in terms of the laser pulse vector potential:

$$\left. \frac{d^2 \tilde{I}}{d\omega d\Omega} \right|_{\theta=0} = \tilde{\kappa} \frac{\omega^2}{4\pi^2} \left| \int_{-\infty}^{+\infty} \mathbf{n} \times [\mathbf{n} \times \mathbf{a}_{\perp}(\eta)] e^{i\omega[\eta + \int_{-\infty}^{\eta} a_{\perp}^2(\eta') d\eta']} d\eta \right|^2. \quad (10)$$

For a circularly polarized laser pulse, the laser pulse vector potential can be expressed as

$$\mathbf{a}_{\perp}(\eta) = \frac{1}{2} a(\eta) \boldsymbol{\varepsilon} e^{i\phi(\eta)} + \text{c.c.}, \quad (11)$$

where  $a(\eta)$  is the envelope function of the pulse,  $\boldsymbol{\varepsilon} = \mathbf{e}_x + i\mathbf{e}_y$  is introduced to take into account circular polarization and  $\phi(\eta)$  is the time-dependent laser pulse phase. We will call  $\omega_i(\eta) = \frac{d\phi}{d\eta}$  instantaneous frequency of the pulse. In the case of a laser pulse with constant frequency  $\omega_0$ , the laser pulse phase is simply given by  $\phi(\eta) = \omega_0 \eta$ . Due to our choice of units,  $\omega_0 = 1$ , but we keep it in these equations to facilitate

consideration of cases with chirped laser pulses, or cases, where laser pulses with different colors are used.

As an illustrative example, expressions for the on-axis spectrum can be obtained in the fully nonlinear case for a laser pulse having an envelope in time described by a half-sine profile:

$$a(\eta) = a_0 \sin \left[ \frac{\pi \eta}{\tau_L} \right], \quad 0 < \eta < \tau_L, \quad (12)$$

with  $\tau_L$  being the dimensionless duration of the laser pulse (such that  $\tau_L/2\pi$  gives the duration of the laser pulse in terms of laser cycles). We have analytically and numerically checked that using other laser pulse envelopes leads to similar results [41,46]. For a pulse, with the envelope given by Eq. (12), the  $z$  coordinate of the electron can be analytically found from Eq. (8):

$$z(\eta) = \frac{a_0^2}{4} \left( \eta - \frac{\tau_L}{2\pi} \sin \frac{2\pi \eta}{\tau_L} \right). \quad (13)$$

The on-axis spectrum of reflected radiation can then be rewritten in the following form:

$$\left. \frac{d^2 \tilde{I}}{d\omega d\Omega} \right|_{\theta=0} = \tilde{\kappa} \frac{\omega^2}{\omega_0^2} \frac{a_0^2}{2\pi^2} N_0^2 \times \left| \int_0^{2\pi} \sin \left( \frac{\xi}{2} \right) \sin(N_0 \xi) e^{i\rho N_0 \xi - i\chi \sin \xi} d\xi \right|^2, \quad (14)$$

where

$$N_0 = \frac{\omega_0 \tau_L}{2\pi}, \quad \chi = \frac{\omega a_0^2 \tau_L}{4\pi}, \quad \rho = \frac{\omega}{\omega_0} \left( 1 + \frac{a_0^2}{2} \right). \quad (15)$$

Numerical integration of these equations can be used to show the dependence of the spectrum on  $a_0$ , as illustrated by a color-coded image of the on-axis spectrum in Fig. 2 (left). The spectra are obtained from numerical integration of Eq. (14) for different  $a_0$  (vertical axis) and for laser pulse with duration  $\tau_L = 600$ . One can see that for low values of  $a_0$  the spectrum is narrow and is limited by the bandwidth of the incoming electromagnetic wave, whereas for large values of  $a_0$  the spectrum is broad and band substructure is visible. The main peak of the spectrum is redshifted and its position is given by Eq. (1) [shown with the dashed line in the Fig. 2 (left)].

While numerical integration of the nonlinear spectrum has been conducted previously, analytic solutions are important to allow understanding of the mechanisms of broadening and to allow design of techniques to compensate for broadening. Opening the sine functions using Euler's formula, one can analytically evaluate the integral to obtain directly the nonlinear spectrum. Doing so yields

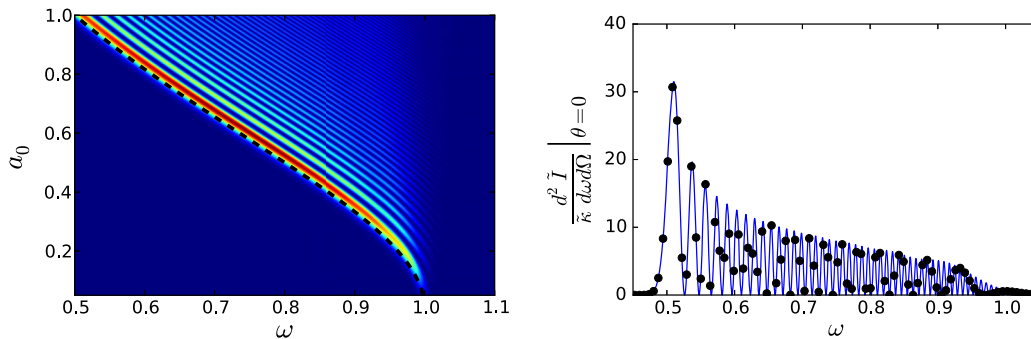


FIG. 2. Left: On-axis radiation spectra plotted as a function of laser pulse amplitude  $a_0$  (vertical axis). The spectra are in arbitrary units, from numerical integration of Eq. (14). Laser pulse duration is  $\tau_L = 600$ . The dashed black line represents the redshift of the peak of the spectrum according to Eq. (1). Right: On-axis radiation spectrum for  $a_0 = 1$  from the analytical expression of Eq. (16) (black circles) for such frequencies as make the order of the Bessel function given by Eq. (17) an integer, overplotted with the full spectrum from numerical integration (blue line).

$$\left. \frac{d^2 \tilde{I}}{d\omega d\Omega} \right|_{\theta=0} = \tilde{\kappa} \left( \frac{\omega}{\omega_0} \right)^2 \frac{a_0^2}{8} N_0^2 |J_n(\chi) - J_{n-1}(\chi)|^2, \quad (16)$$

where  $J_n$  is the Bessel function and

$$n = N_0(\rho - 1) + \frac{1}{2}. \quad (17)$$

Here we have neglected two small terms that are given by Bessel functions with orders  $N_0(\rho + 1) \pm \frac{1}{2}$  because  $N_0 \gg 1$  typically for  $\tau_L \gg 2\pi/\omega_0$ , and Bessel functions with such orders are very small in the frequency range of interest. It is important to note that the solution is valid only for a subset of all  $\omega$  where the order  $n$  is an integer.<sup>1</sup> For other values of  $\omega$ , numerical integration of Eq. (14) is required. Figure 2 (right) displays the spectrum for  $a_0 = 1$  and laser pulse with duration  $\tau_L = 600$ . Black dots show the analytical solution from Eq. (16) for the frequencies  $\omega$  that make the order  $n$  an integer. One can see that analytical solution fits the numerical integration (blue line) very well. Although the analytical solution provides only a discrete set of points, it well outlines the shape of the spectrum and gives its peak value and width which are the most important parameters for many applications. This is especially true because in many Thomson scattering photon source applications the fine-scale oscillations observable for a single electron will be washed out by the nonzero energy spread of the electron beam. In the example shown here, the oscillations have frequency spacing of  $\approx 2\% \omega_0$  which will be washed out by electron energy spread of  $\approx 1\%$ . The analytic expressions then allow us to analytically evaluate broadening, and give us a tool to calculate compensating terms which can be used to control and narrow the spectrum.

<sup>1</sup>In principle the integral in Eq. (14) is one of the Schlöfli's integrals, but for simplicity we keep Bessel functions instead. This does not change the results of the paper.

### III. CONTROLLING THE SHAPE OF THE SPECTRUM BY LASER PULSE CHIRPING

Nonlinear broadening of the spectrum is a result of redshifting of the Thomson scattered frequency during the interaction due to the longitudinal motion of the electron, as given by Eq. (2) with the laser pulse envelope. This indicates that by compensating the laser frequency by chirping the laser pulse, one can diminish broadening of the generated spectrum. This was proposed, and simulation based on a single set of numerical parameters was provided in [35], and further examples were provided in [47]. Here we extend the analytical expressions obtained above to derive analytical expressions for the radiation spectrum in the case of proper laser pulse chirping. Using appropriate laser chirp, spectrum narrowing can be obtained for high values of laser pulse amplitude  $a_0 > 1$ . The analytical results are compared with numerical integration.

We consider again the circularly polarized laser pulse with the envelope given by Eq. (12). If the frequency of the laser pulse is constant the generated frequency is given by Eq. (2), and the resulting spectra are those of Fig. 2. However, if the instantaneous frequency of the laser pulse is given by

$$\omega_i(\eta) = [1 + a(\eta)^2], \quad (18)$$

then the reflected radiation frequency will be constant and equal to unity independent of the value of  $a_0$ . This can be derived from the following considerations. Substituting Eq. (11) into Eq. (10) and examining the oscillatory term of the integral  $e^{i\Phi(\eta)}$ , one can write the phase as

$$\Phi(\eta) = -\phi(\eta) + \omega\eta + \omega \int_{-\infty}^{\eta} a_{\perp}^2(\eta') d\eta'. \quad (19)$$

The time-dependent laser pulse phase  $\phi(\eta)$  will compensate for the redshifting and yield the maximum of the integral at  $\omega = 1$ , provided  $\Phi(\eta)$  is constant at  $\omega = 1$ . Thus,

$$-\phi(\eta) + \eta + \int_{-\infty}^{\eta} a_{\perp}^2(\eta') d\eta' = C. \quad (20)$$

For the phase of the properly chirped laser pulse one can thus write

$$\phi(\eta) = \eta + \int_{-\infty}^{\eta} a_{\perp}^2(\eta') d\eta' - C, \quad (21)$$

and for the instantaneous laser pulse frequency one obtains the following expression:

$$\omega_i(\eta) = \frac{d\phi(\eta)}{d\eta} = 1 + a_{\perp}^2(\eta). \quad (22)$$

Note that in the case of the circularly polarized laser pulse, Eq. (22) coincides with Eq. (18). The case of linear polarization has been considered in [52] and the results are similar. For the laser pulse with envelope given by Eq. (12) and instantaneous frequency given by Eq. (22) one can derive an analytical solution. Note that the longitudinal coordinate of the electron is still given by Eq. (13) as the laser pulse is chosen to be circular. The result of the spectrum calculation using Eq. (9) yields the same formula as in Eq. (16), but with  $n$  and  $\chi$  given by

$$n = (\omega - 1)N_0 \left(1 + \frac{a_0^2}{2}\right) + \frac{1}{2} \quad (23)$$

$$\chi = \frac{1 - \omega}{2} N_0. \quad (24)$$

The analytical solutions for the nonlinear spectral bandwidth using a laser pulse with the envelope given by Eq. (12) and instantaneous frequency given by Eq. (18) are shown in Fig. 3 (left), where normalized spectra are presented for different values of  $a_0$ . Markers of different colors show the analytical solutions using Eqs. (16), (23) and (24), while solid lines of corresponding colors show the numerical integration results. Analytical solutions fit with

numerical integration well and predict spectrum narrowing for properly chirped laser pulses with high values of  $a_0$ . The generated frequency stays centered at  $\omega = 1$  and the broadening disappears. In the case of  $a_0 = 0.1$  (blue color) the spectrum width is approximately given by the unchirped (i.e., with constant frequency, shown on the figure with black dash-dotted line) laser pulse width, which is inversely proportional to laser pulse duration  $\tau_L$ . One can see that the spectrum is getting narrower with the increase of  $a_0$ . For arbitrary values of  $a_0$ , the spectrum width scales approximately as  $\frac{\Delta\omega}{\omega} \propto \frac{1}{\tau_L(1+a_0^2)}$ , i.e., in the case of  $a_0 = 10$  (black color) the spectrum width is approximately  $a_0^2 = 100$  times narrower. This is due to the choice of the laser pulse function. Indeed, changing (increasing compared to  $\omega = 1$ ) the frequency while keeping the duration  $\tau_L$  constant leads to more periods. This can be seen from Fig. 5 (left) where normalized laser pulse vector potential is plotted for the case when the laser pulse is unchirped (blue color) and for the case of chirped laser pulse with  $a_0 = 0.5$  (green color). In this figure the duration of the laser pulse was set to  $\tau_L = 60$  for illustrative reasons. Because at each period an electron is forced (by appropriate chirp) to radiate the same frequency, it effectively radiates pulses with the same frequency  $\omega = 1$  but with longer duration for higher  $a_0$  leading to a narrower emitted spectrum. Numerical integration of the generated spectra using Eq. (9) is presented in Fig. 3 (right). The color-coded image is the normalized on-axis spectrum (in logarithmic scale) as a function of both the frequency (longitudinal axis) and normalized laser amplitude  $a_0$  (vertical axis) similar to Fig. 2 (left). Results are normalized to the peak value of the spectrum for  $a_0 = 10$ , demonstrating the scaling of the peak value of the spectrum with  $a_0$ . Though throughout the paper classical description has been used, it is interesting to analyze the scaling of the peak value of the photon on-axis spectrum, which is given by

$$\left. \frac{d^2 N_{\text{ph}}}{d\omega d\Omega} \right|_{\theta=0} = \alpha \frac{\omega}{\omega_0^2} \frac{a_0^2}{8} N_0^2 |J_n(\chi) - J_{n-1}(\chi)|^2, \quad (25)$$

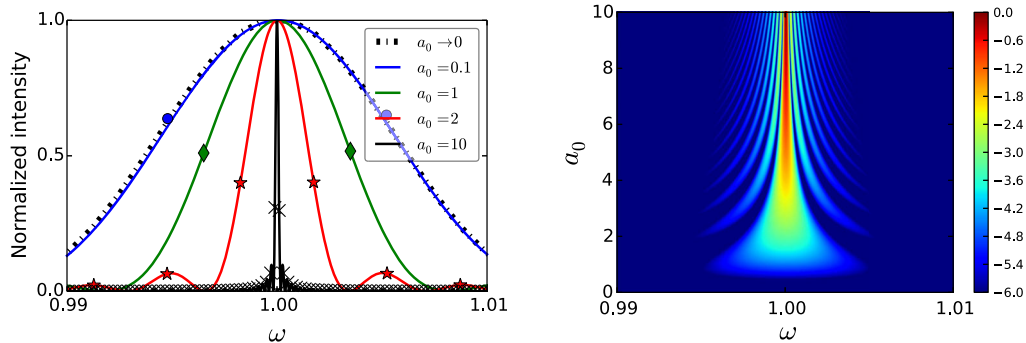


FIG. 3. Left: Normalized on-axis intensity spectra for different values of  $a_0$  for the case of a laser pulse with duration  $\tau_L = 600$ . Laser pulse is properly chirped according to Eq. (18). Results obtained with the help of numerical integration are shown with solid lines. Markers of corresponding color present the analytical solution using Eqs. (16), (23) and (24). Right: Numerically obtained on-axis radiation spectra for a properly chirped laser pulse for different values of  $a_0$  (vertical axis) in the logarithmic scale.

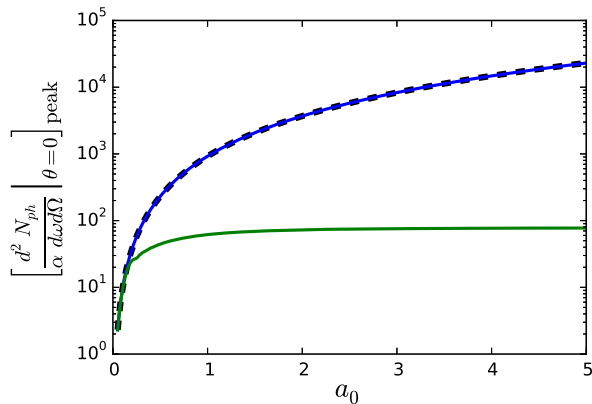


FIG. 4. Peak value of the on-axis photon spectrum as a function of  $a_0$  for the cases of unchirped (green solid line) and properly chirped (blue solid and black dashed lines) pulses. The black dashed line represents the fit to the numerical data given by Eq. (26).

with the values of  $n$  and  $\chi$ , corresponding to the chirped or unchirped case. Here,  $N_{\text{ph}}$  is the number of photons and  $\alpha \approx 1/137$  is the fine-structure constant. The peak value of the on-axis photon spectrum as a function of  $a_0$  for the laser pulse with duration  $\tau_L = 600$  and obtained numerically, is presented in Fig. 4 for the cases of unchirped pulse (green line) and properly chirped pulse (blue solid and black dashed lines). One can see that, in the case of the unchirped pulse, the peak value of the on-axis photon spectrum saturates and is independent of  $a_0$  for  $a_0 \gg 1$ . Contrary, in the case of the chirped pulse, the peak value of the on-axis photon spectrum grows proportionally to  $a_0^2$  as shown by the blue solid line. Black dashed line represents a fit to the numerically obtained peak value of the on-axis spectrum for the case of the chirped pulse, which is given by

$$\left[ \frac{d^2 N_{\text{ph}}}{\alpha d\omega d\Omega} \Big|_{\theta=0} \right]_{\text{peak}} = \alpha \frac{a_0^2 \tau_L^2}{4\pi^4}. \quad (26)$$

Exact fit coefficients will depend on the pulse shape, but the  $a_0^2$  scaling will stay the same. In the paper by Seipt *et al.*

[52], the off-axis spectrum was also analyzed. Even though for different observation angles the ponderomotive broadening is not exactly compensated, the total number of photons in the natural bandwidth, which is equal to the laser pulse bandwidth  $\frac{\Delta\omega_L}{\omega_L}$ , was estimated to be

$$N_{\text{ph,nat}} \approx \pi\alpha a_0^2. \quad (27)$$

This justifies one more time the benefits of using properly chirped pulses for obtaining narrow bandwidth photon sources.

It is worth noting that the spectrum of the incident chirped pulse extends approximately up to the frequency  $\omega_{\text{max}} = (1 + a_0^2)$ , quadratic with  $a_0$ . Figure 5 (right) shows the normalized spectra of laser pulses properly chirped according to Eq. (18) (red color corresponds to  $a_0 = 0.2$  and green color corresponds to  $a_0 = 0.5$ ) compared to the case of the unchirped laser pulse. For low values of  $a_0 < 1$  the introduced chirp can be on the order of 10–20 percent and is achievable with current technology. This already allows production of narrow bandwidth sources using significantly higher laser intensity than is conventionally possible, which in turn reduces the required laser energy. As noted above, even operation at  $a_0 = 0.3$  compared to  $a_0 = 0.15$  can save a factor of 4 in scattering laser energy. While in principle the technique can be used up to even higher intensities, practical implementation is limited by the obtainable bandwidth in the scattering laser. For example, at  $a_0 = 10$  the laser pulse contains the range of wavelengths from x rays to the laser wavelength, which is beyond currently foreseeable laser technology.

#### IV. CONCLUSIONS

In this paper we have presented analytical solutions for the on-axis spectrum of radiation generated by a free electron interacting with a plane circularly polarized laser pulse of nonlinear intensity. Discussion of effects of laser pulse spatial structure, off-axis spectrum calculations and simulations using realistic electron beams can be found in

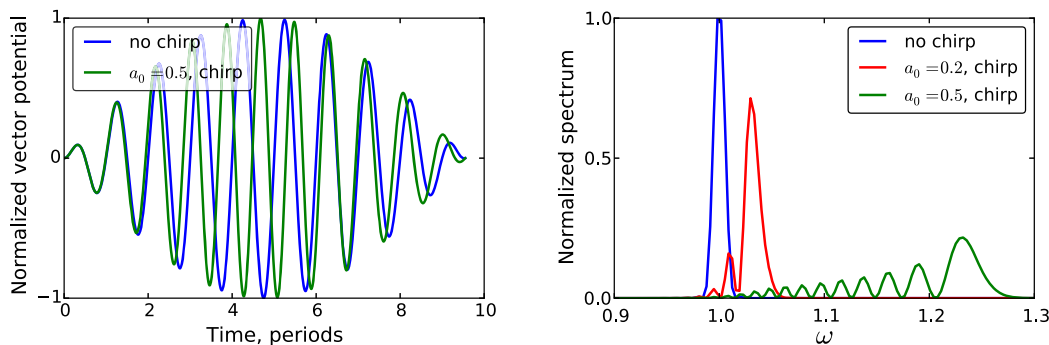


FIG. 5. Left: Normalized vector potential as a function of time in periods for the case of the unchirped laser pulse (blue color) and chirped laser pulse with  $a_0 = 0.5$  for laser pulse with duration  $\tau_L = 60$ . Right: Laser pulse spectra (normalized to the peak value of the unchirped pulse spectrum) for the case of unchirped laser pulse (blue color) and chirped laser pulses with  $a_0 = 0.2$  (red color) and  $a_0 = 0.5$  (green color) for laser pulse with duration  $\tau_L = 600$ .

Ref. [52]. The results presented in this paper are derived for an electron initially at rest for computational clarity. They apply also, using a straightforward Lorentz transform into the beam frame, to Thomson scattering sources of x rays and gamma rays which scatter laser pulses from relativistic electron beams. The analytical results agree very well with results of numerical integration and provide useful insights and scalings for nonlinear Thomson scattering. We have shown analytically and numerically that by proper chirping of the laser pulse the broadening of the radiation spectrum can be avoided for high values of laser pulse amplitude  $a_0 > 1$ . The results predict laser amplitude and pulse shape parameters to compensate nonlinear broadening and produce narrow bandwidth sources at high intensity. This result is important for generation of high flux Thomson scattering sources of x rays and gamma rays, as it allows generation of a given photon flux using greatly reduced laser energy. Moreover, the results presented in this paper can be used for optimization of experiments as well as benchmarking of the numerical tools.

### ACKNOWLEDGMENTS

This work was supported by the U.S. Department of Energy National Nuclear Security administration DNN R&D/NA-22, and by the Office of Science Office of High Energy Physics, under Contract No. DE-AC02-05CH11231. The simulations used the resources of the National Energy Research Scientific Computing Center, a DOE Office of Science User Facility supported by the Office of Science of the U.S. Department of Energy under Contract No. DE-AC02-05CH11231. S. G. R. would like to acknowledge support from Helmholtz Association (Helmholtz Young Investigators group VH-NG-1037). We would like to acknowledge fruitful discussions with M. Zolotarev, M. Efremov, C. Benedetti, D. Seipt and V. Kharin.

- 
- [1] P. Sprangle, A. Ting, E. Esarey, and A. Fisher, Observation of 20 eV x-ray generation in a proof-of-principle laser synchrotron source experiment, *J. Appl. Phys.* **78**, 575 (1992).
  - [2] E. Esarey, S. K. Ride, and P. Sprangle, Nonlinear Thomson scattering of intense laser pulses from beams and plasmas, *Phys. Rev. E* **48**, 3003 (1993).
  - [3] R. W. Schoenlein, W. P. Leemans, A. H. Chin, P. Volfbeyn, T. E. Glover, P. Balling, M. Zolotarev, K.-J. Kim, S. Chattopadhyay, and C. V. Shank, Femtosecond x-ray pulses at 0.4 Å generated by 90 Thomson scattering: A tool for probing the structural dynamics of materials, *Science* **274**, 236 (1996).
  - [4] W. P. Leemans, R. W. Schoenlein, P. Volfbeyn, A. H. Chin, T. E. Glover, P. Balling, M. Zolotarev, K. J. Kim, S. Chattopadhyay, and C. V. Shank, X-Ray Based Subpicosecond Electron Bunch Characterization Using 90 degrees Thomson Scattering, *Phys. Rev. Lett.* **77**, 4182 (1996).
  - [5] K. Achterhold, M. Bech, S. Schleede, G. Potdevin, R. Ruth, R. Loewen, and F. Pfeiffer, Monochromatic computed tomography with a compact laser-driven x-ray source, *Sci. Rep.* **3**, 1313 (2013).
  - [6] F. Albert, S. G. Anderson, D. J. Gibson, C. A. Haggmann, M. S. Johnson, M. Messerly, V. Semenov, M. Y. Shverdin, B. Rusnak, A. M. Tremaine, F. V. Hartemann, C. W. Siders, D. P. McNabb, and C. P. J. Barty, Characterization and applications of a tunable, laser-based, MeV-class Compton-scattering  $\gamma$ -ray source, *Phys. Rev. ST Accel. Beams* **13**, 070704 (2010).
  - [7] F. R. Arutyunyan and V. A. Tumanyan, Quasimonochromatic and polarized high-energy gamma rays, *Phys. Usp.* **7**, 339 (1964).
  - [8] E. Bulyak, P. Gladkikh, and A. Zelinsky, Compact x-ray source based on Compton backscattering, *Nucl. Instrum. Methods Phys. Res., Sect. A* **487**, 241 (2002).
  - [9] J. Chen, K. Imasaki, and M. Fujita, Development of a compact high brightness x-ray source, *Nucl. Instrum. Methods Phys. Res., Sect. A* **341**, 346 (1994).
  - [10] F. V. Hartemann, D. J. Gibson, and W. J. Brown, Compton scattering x-ray sources driven by laser wakefield acceleration, *Phys. Rev. ST Accel. Beams* **10**, 11301 (2007).
  - [11] K. Kawase and M. Kando, Sub-MeV tunably polarized x-ray production with laser Thomson backscattering, *Rev. Sci. Instrum.* **79**, 053302 (2008).
  - [12] O. F. Kulikov, Y. Y. Telnov, E. I. Filippov, and M. N. Yakimenko, Compton effect on moving electrons, *Phys. Lett.* **13**, 344 (1964).
  - [13] V. N. Litvinenko and J. M. J. Madey, Intense Compton  $\gamma$ -ray source from the Duke storage ring FEL, *Nucl. Instrum. Methods Phys. Res., Sect. A* **375**, 580 (1996).
  - [14] V. G. Nedorezov, A. A. Turinge, and Y. M. Shatunov, Photonuclear experiments with Compton-backscattered gamma beams, *Phys. Usp.* **47**, 341 (2004).
  - [15] H. Ohgaki, T. Noguchi, and S. Sugiyama, Linearly polarized photons from Compton backscattering of laser light for nuclear resonance fluorescence experiments, *Nucl. Instrum. Methods Phys. Res., Sect. A* **353**, 384 (1994).
  - [16] I. V. Pogorelsky, I. Ben-Zvi, X. J. Wang, and T. Hirose, Femtosecond laser synchrotron sources based on Compton scattering in plasma channels, *Nucl. Instrum. Methods Phys. Res., Sect. A* **455**, 176 (2000).
  - [17] E. S. Sarachik and G. T. Schappert, Classical theory of the scattering of intense laser radiation by free electrons, *Phys. Rev. D* **1**, 2738 (1970).
  - [18] H. Schwoerer, B. Liesfeld, H.-P. Schlenvoigt, K.-U. Amthor, and R. Sauerbrey, Thomson-Backscattered X Rays From Laser-Accelerated Electrons, *Phys. Rev. Lett.* **96**, 014802 (2006).
  - [19] F. Villa, A. Luccio, and M. Zolotarev, A source of kilovolt x-ray, *Microsyst. Technol.* **2**, 79 (1996).
  - [20] K. Khrennikov, J. Wenz, A. Buck, J. Xu, M. Heigoldt, L. Veisz, and S. Karsch, Tunable All-Optical Quasimonochromatic Thomson X-Ray Source in the Nonlinear Regime, *Phys. Rev. Lett.* **114**, 195003 (2015).
  - [21] G. Sarri, D. J. Corvan, W. Schumaker, J. M. Cole, A. Di Piazza, H. Ahmed, C. Harvey, C. H. Keitel, K. Krushelnick, S. P. D. Mangles, Z. Najmudin, D. Symes, A. G. R. Thomas,

- M. Yeung, Z. Zhao, and M. Zepf, Ultrahigh Brilliance Multi-MeV  $\gamma$ -Ray Beams from Nonlinear Relativistic Thomson Scattering, *Phys. Rev. Lett.* **113**, 224801 (2014).
- [22] N. D. Powers, I. Ghebregziabher, G. Golovin, C. Liu, S. Chen, S. Banerjee, J. Zhang, and D. P. Umstadter, Quasimonoeenergetic and tunable x-rays from a laser-driven Compton light source, *Nat. Photonics* **8**, 28 (2014).
- [23] F. Albert, S. G. Anderson, and D. J. Gibson, Design of narrow-band Compton scattering sources for nuclear resonance fluorescence, *Phys. Rev. ST Accel. Beams* **14**, 050703 (2011).
- [24] W. Bertozzi, J. Caggiano, W. Hensley, M. Johnson, S. Korbly, R. Ledoux, D. McNabb, E. Norman, W. Park, and G. Warren, Nuclear resonance fluorescence excitations near 2 MeV in U235 and Pu239, *Phys. Rev. C* **78**, 041601 (2008).
- [25] C. G. R. Geddes, S. G. Rykovanov, N. H. Matlis, S. Steinke, J.-L. Vay, E. Esarey, B. Ludewigt, K. Nakamura, B. J. Quiter, C. B. Schroeder, C. Toth, and W. P. Leemans, Compact quasimonoeenergetic photon sources from laser-plasma accelerators for nuclear detection and characterization, *Nucl. Instrum. Methods Phys. Res., Sect. B* **350**, 116 (2015).
- [26] B. J. Quiter, B. A. Ludewigt, V. V. Mozin, C. Wilson, and S. Korbly, Transmission nuclear resonance fluorescence measurements of 238U in thick targets, *Nucl. Instrum. Methods Phys. Res., Sect. B* **269**, 1130 (2011).
- [27] S. G. Rykovanov, C. G. R. Geddes, J. L. Vay, C. B. Schroeder, E. Esarey, and W. P. Leemans, Quasimonoeenergetic femtosecond photon sources from Thomson scattering using laser plasma accelerators and plasma channels, *J. Phys. B* **47**, 234013 (2014).
- [28] B. J. Quiter, S. G. Prussin, B. Pohl, J. Hall, J. Trebes, G. Stone, and M.-A. Descalle, A method for high-resolution x-ray imaging of intermodal cargo containers for fissionable materials, *J. Appl. Phys.* **103**, 064910 (2008).
- [29] R. Tommasini, S. P. Hatchett, D. S. Hey, C. Iglesias, N. Izumi, J. A. Koch, O. L. Landen, A. J. MacKinnon, C. Sorce, J. A. Delettrez, V. Yu. Glebov, T. C. Sangster, and C. Stoeckl, Development of Compton radiography of inertial confinement fusion implosions, *Phys. Plasmas* **18**, 056309 (2011).
- [30] F. E. Carroll, M. H. Mendenhall, R. H. Traeger, C. Brau, and J. W. Waters, Pulsed tunable monochromatic x-ray beams from a compact source: New opportunities, *Am. J. Roentgenol.* **181**, 1197 (2003).
- [31] K. J. Weeks, V. N. Litvinenko, and J. M. Madey, The Compton backscattering process and radiotherapy, *Med. Phys.* **24**, 417 (1997).
- [32] E. Esarey, C. Schroeder, and W. Leemans, Physics of laser-driven plasma-based electron accelerators, *Rev. Mod. Phys.* **81**, 1229 (2009).
- [33] Y. Ding, A. Brachmann, F.-J. Decker, D. Dowell, P. Emma, J. Frisch, S. Gilevich, G. Hays, Ph. Hering, Z. Huang, R. Iverson, H. Loos, A. Miahnahri, H.-D. Nuhn, D. Ratner, J. Turner, J. Welch, W. White, and J. Wu, Measurements and Simulations of Ultralow Emittance and Ultrashort Electron Beams in the Linac Coherent Light Source, *Phys. Rev. Lett.* **102**, 254801 (2009).
- [34] C. Brau, Oscillations in the spectrum of nonlinear Thomson-backscattered radiation, *Phys. Rev. ST Accel. Beams* **7**, 020701 (2004).
- [35] I. Ghebregziabher, B. A. Shadwick, and D. Umstadter, Spectral bandwidth reduction of Thomson scattered light by pulse chirping, *Phys. Rev. ST Accel. Beams* **16**, 030705 (2013).
- [36] F. V. Hartemann and S. S. Q. Wu, Nonlinear Brightness Optimization in Compton Scattering, *Phys. Rev. Lett.* **111**, 044801 (2013).
- [37] F. V. Hartemann, F. Albert, C. W. Siders, and C. P. J. Barty, Low-Intensity Nonlinear Spectral Effects in Compton Scattering, *Phys. Rev. Lett.* **105**, 130801 (2010).
- [38] F. V. Hartemann, A. L. Troha, N. C. Luhmann, and Z. Toffano, Spectral analysis of the nonlinear relativistic Doppler shift in ultrahigh intensity Compton scattering, *Phys. Rev. E* **54**, 2956 (1996).
- [39] T. Heinzl, D. Seipt, and B. Kämpfer, Beam-shape effects in nonlinear Compton and Thomson scattering, *Phys. Rev. A* **81**, 022125 (2010).
- [40] D. Seipt and B. Kämpfer, Nonlinear Compton scattering of ultrashort intense laser pulses, *Phys. Rev. A* **83**, 022101 (2011).
- [41] D. Seipt, V. Kharin, S. G. Rykovanov, A. Surzhykov, and S. Fritzsche, Analytical results for nonlinear Compton scattering in short intense laser pulses, [arXiv:1601.00442](https://arxiv.org/abs/1601.00442).
- [42] S. P. Goreslavskii, S. V. Popruzhenko, and O. V. Shcherbachev, The angular distribution of nonlinear Thomson scattering in a circular field, *Laser Phys.* **9**, 1039 (1999).
- [43] M. Boca and V. Florescu, Thomson and Compton scattering with an intense laser pulse, *Eur. Phys. J. D* **61**, 449 (2011).
- [44] G. A. Krafft, Spectral Distributions of Thomson-Scattered Photons from High-Intensity Pulsed Lasers, *Phys. Rev. Lett.* **92**, 204802 (2004).
- [45] C. Maroli, V. Petrillo, P. Tomassini, and L. Serafini, Nonlinear effects in Thomson backscattering, *Phys. Rev. ST Accel. Beams* **16**, 030706 (2013).
- [46] V. Kharin, D. Seipt, and S. G. Rykovanov, Temporal laser pulse shape effects in nonlinear Thomson scattering, [arXiv:1602.03062](https://arxiv.org/abs/1602.03062).
- [47] B. Terzić, K. Deitrick, A. S. Hofler, and G. A. Krafft, Narrow-Band Emission in Thomson Sources Operating in the High-Field Regime, *Phys. Rev. Lett.* **112**, 074801 (2014).
- [48] A. I. Nikishov and V. I. Ritus, Quantum processes in the field of a plane electromagnetic wave and in a constant field. I, *Sov. Phys. JETP* **19**, 529 (1964).
- [49] G. Mourou, T. Tajima, and S. Bulanov, Optics in the relativistic regime, *Rev. Mod. Phys.* **78**, 309 (2006).
- [50] J. D. Jackson, *Classical Electrodynamics* (John Wiley & Sons, Inc., New York, 1975).
- [51] L. D. Landau and E. M. Lifshitz, *The Classical Theory of Fields, Fourth Edition: Volume 2*, Course of Theoretical Physics Series (Butterworth-Heinemann, Washington, DC, 1980).
- [52] D. Seipt, S. G. Rykovanov, A. Surzhykov, and S. Fritzsche, Narrowband inverse Compton scattering x-ray sources at high laser intensities, *Phys. Rev. A* **91**, 033402 (2015).